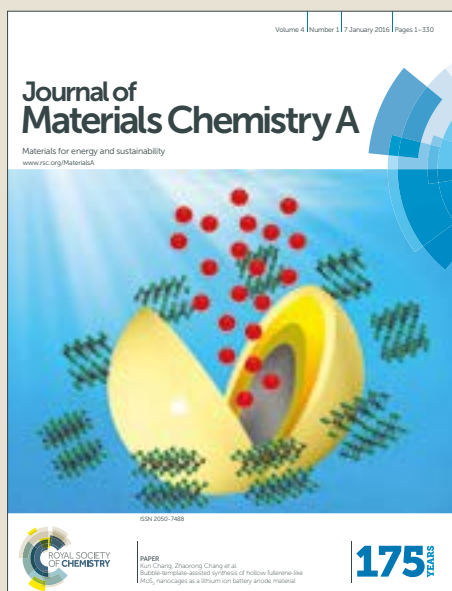


Journal of Materials Chemistry A

Accepted Manuscript



This is an Accepted Manuscript, which has been through the Royal Society of Chemistry peer review process and has been accepted for publication.

Accepted Manuscripts are published online shortly after acceptance, before technical editing, formatting and proof reading. Using this free service, authors can make their results available to the community, in citable form, before we publish the edited article. We will replace this Accepted Manuscript with the edited and formatted Advance Article as soon as it is available.

You can find more information about Accepted Manuscripts in the [author guidelines](#).

Please note that technical editing may introduce minor changes to the text and/or graphics, which may alter content. The journal's standard [Terms & Conditions](#) and the ethical guidelines, outlined in our [author and reviewer resource centre](#), still apply. In no event shall the Royal Society of Chemistry be held responsible for any errors or omissions in this Accepted Manuscript or any consequences arising from the use of any information it contains.



Journal Name

ARTICLE

Multifunctional Poly-N-Vinylcarbazole Interlayer in Perovskite Solar Cells for High Stability and Efficiency: A Test with New Triazatruxene-Based Hole Transporting Materials

Received 00th January 20xx,
Accepted 00th January 20xx

DOI: 10.1039/x0xx00000x

www.rsc.org/

Pei-Yang Su,^a Li-Bo Huang,^a Jun-Min Liu,^{*a} Yi-Fan Chen,^a Li-Min Xiao,^b Dai-Bin Kuang,^a Marcel Mayor,^a and Cheng-Yong Su^{*a}

The hydrophobic and conductive polymer poly-N-vinylcarbazole (PVK) has been successfully utilized as a multifunctional interlayer between perovskite and hole transporting material (HTM) for high stable and efficient perovskite solar cells (PSCs) for the first time. The very thin PVK interlayer can not only protect perovskite structure from moisture and degradation, but also modulate interface to reduce charge recombination and promote hole transportation simultaneously. Beneficial from collaboration of this PVK-protection method with molecular design of an economical and synthetically facile triazatruxene-based HTM (SP-12) featuring good stability, planarity and hole mobility, a reliable power conversion efficiency of 18.8% has been achieved, which is superior to that using the well-studied spiro-OMeTAD (16.9%), demonstrating a promising fabrication approach to efficient and long-term stable PSCs.

Perovskite solar cells (PSCs) are rapidly evolving into a promising technology to convert solar energy into electricity owing to fast increase of power conversion efficiency (PCE) from less than 3.8% to over 20% in the past few years.¹⁻¹⁸ Besides unique optical and electrical properties of the hybrid organo-lead trihalide $\text{CH}_3\text{NH}_3\text{PbX}_3$ (X=Cl, Br, or I) perovskites,¹⁹ the optimization of the cell structure and different layer morphology plays a key role in achieving high performance, which is strongly related to the material composition and processing conditions.²⁰⁻²² The long-term stability remains a great challenge for PSCs, particularly when subjected to environmental stresses such as moisture,²³ under which the device deteriorates quickly.²⁴ Therefore, deliberate attempts have been made to replace the CH_3NH_3 group with a more stable unit²⁵ or to utilize hydrophobic HTMs to improve moisture resistance,²⁶ but little attention was paid to introduce a polymeric interlayer which could play a protective role by shielding volatile perovskites from atmospheric moisture.

On the other hand, the hole-transport materials (HTMs), which separate photo-excited electron-hole pairs and transport the holes to the external circuit, represent another important factor determining device performance.²⁷ Among various promising HTMs so far reported,²⁸ the triarylamine-based 2,2',7,7'-tetrakis(N,N-di-*p*-methoxyphenylamine)-9,9'-spiro-bifluorene (spiro-OMeTAD) is the

most effective one.²⁹ However, the tedious synthesis and purification steps make it expensive for large-scale application.³⁰ Very recently, a new class of star-shaped triazatruxene-based HTMs was reported as a low-cost but effective alternative of spiro-OMeTAD,³¹⁻³² in which long *n*-hexyl chains are attached to make it soluble and protect perovskite surface from moisture. Based on the present research in perovskite solar cells, perovskite layer could hardly cover the surface of the TiO_2 layer totally.³³⁻³⁴ Therefore, the uncovered traps on TiO_2 layer could be in contact with HTMs directly, resulting in electron recombination from the conduction band of TiO_2 to HTMs.³⁵

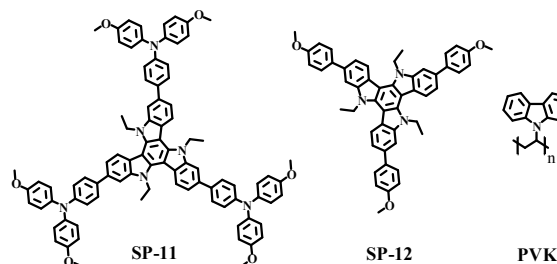


Fig. 1 Chemical structures of SP-11, SP-12 and PVK.

To solve these problems, herein we propose a new protection approach by introducing a thin polymer interlayer featuring hydrophobicity and conductivity in between perovskite and HTM to resist moisture and suppress charge recombination simultaneously. As a widely used conductive organic polymer, poly-N-vinylcarbazole (PVK) is proven to be effective as hole carrier in photorefractive applications³⁶⁻³⁸ and organic solar cells.³⁹⁻⁴¹ However, PVK as polymer interlayer between perovskite and HTM of PSCs has never

^a MOE Laboratory of Bioinorganic and Synthetic Chemistry, Lehn Institute of Functional Materials, School of Chemistry, and School of Materials Science and Engineering, Sun Yat-sen University, Guangzhou 510275, China. *E-mail: cecssy@mail.sysu.edu.cn; liujunm@mail.sysu.edu.cn

^b School of Computer Science and Engineering, Beihang University, Beijing 100191, China.

† Electronic supplementary information (ESI) available: Experimental details including synthesis, experimental procedure and supporting data. See DOI: 10.1039/x0xx00000x.

been reported. Considering PVK is hydrophobic and characteristic of good film formation, incorporation of PVK-protection interlayer may benefit interfacial modulation instead of direct contact of perovskite with hydrophobic chains deliberately attached to HTMs. Therefore, new triazatruxene-based derivatives, 2,7,12-tris(4-methoxyphenyl)-5,10,15-triethyltriindole (**SP-11**) and 2,7,12-tris(N,N-bis(4-methoxyphenyl)aniline)-5,10,15-triethyltriindole (**SP-12**), are designed to attach short ethyl groups into 2,7,12-positions of the triazatruxene aromatic core (Fig. 1), in order to preserve its two-dimensional planar π -system to facilitate intermolecular charge transfer. **SP-11** and **SP-12** are soluble in common organic solvents, and thus integration of a perovskite/PVK/HTM multiply layer can be performed *via* a convenient solution process. The optimized devices reach PCE as high as 18.8%, offering a new direction of processing method for stable and efficient PCSs by means of introducing multifunctional polymer interlayer in devices.

To investigate the protection effect of PVK layer on PSCs, planar perovskite solar cells based on the structure of FTO/compact-TiO₂/CH₃NH₃PbI₃/PVK/spiro-OMeTAD/Au with a 580 nm FTO glass and 50 nm Au layer, are designed for the first time, in which sequential deposition of a 240 nm CH₃NH₃PbI₃ layer from precursors PbCl₂ and CH₃NH₃I,⁴² a 10 nm PVK layer sandwiched between perovskite and spiro-OMeTAD, and a 240 nm spiro-OMeTAD layer is performed by spin-coating (Fig. 2). For comparison, a similar device using spiro-OMeTAD alone is also fabricated. The scanning electron microscope (SEM) is employed to observe the morphology of PVK on perovskite at different deposition concentrations (Fig. S1). When spin-coated by 4 mg/mL PVK, the perovskite layer is only partially covered. Increasing PVK concentration to 8 mg/mL, a continuous and uniform PVK film on perovskite top is formed, implying close matching of PVK surface tension with perovskite surface energy. Further increase in concentration to 12 mg/mL results in a thicker but uneven PVK film, while a concentration of 16 mg/mL leads to overwhelmed rough PVK film. Hence, the optimized concentration of PVK is selected at 8 mg/mL.

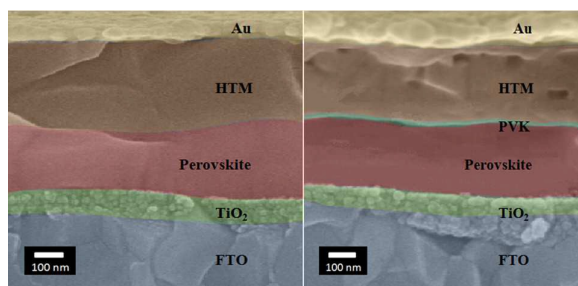


Fig. 2 Cross-sectional SEM images of the planar PSCs containing spiro-OMeTAD alone (left) and PVK interlayer (right). The individual layers have been colored to improve visibility.

The influence of hydrophobic nature of PVK on perovskite layer is examined by the contact angles (α) of deionized water on the different perovskite surfaces (Fig. 3). Pure perovskite films show a rather small α , indicative of easy infiltration of water molecules into the perovskite layer. After coating a PVK film, a big α of 100.7° is obtained, confirming effective modification of the polar character

of the perovskite surface. In comparison with the perovskite film only covered by spiro-OMeTAD, which shows a α of 82.1° with obvious water affinity, introduction of a PVK interlayer between perovskite and spiro-OMeTAD increases α to 96.2°, apparently changing perovskite surface from hydrophilicity to hydrophobicity, thereof effectively preventing water penetration to improve moisture stability of the whole cell.

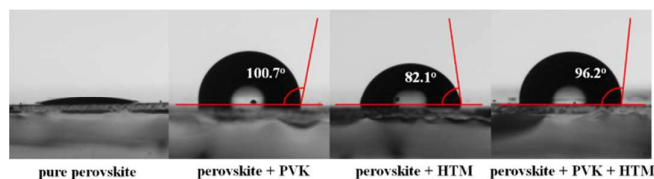


Fig. 3 Water contact angles on the perovskite surfaces under different conditions.

The protective impact of PVK layer on degradation of perovskite has been verified by comparing the color alteration and X-ray diffraction patterns of different films (pure perovskite, pure PVK, perovskite/PVK, perovskite/spiro-OMeTAD, and perovskite/PVK/spiro-OMeTAD, see Fig. S2) exposed to ambient air. The color change from dark brown to yellow is believed to associate with perovskite degradation initiated by infiltration of water molecules to form weak hydrogen bonds with hygroscopic methylammonium cations, leading to bond dissociation between the crystal constituents and liberating unbound methylammonium iodide to leave behind a residual layer of PbI₂.²³ As seen from Fig. S2, the degradation of pure perovskite film progresses significantly within 96 h, when the color turns to pale yellow and the XRD patterns largely transfer to PbI₂. For perovskite/spiro-OMeTAD film, discernible color change is retarded to 96 h but the transition to PbI₂ is obvious in XRD pattern. In contrast, the perovskite film coated with PVK displays much slower degradation with little color alteration and phase change of only small portion in 96 h. Similar slow degradation is observed for perovskite/PVK/spiro-OMeTAD film, indicating that the hydrophobic PVK interlayer plays a significant role in shielding the perovskite structure from atmospheric moisture, thus preventing its degradation.

Fig. 4a shows the current-voltage (*J-V*) curves reflecting the influence of PVK interlayers coated at different concentrations on the performance of corresponding PSCs. A striking finding is that, compared with the pristine spiro-OMeTAD-based device, all characteristic parameters of the PVK/spiro-OMeTAD-based cells are generally enhanced (Table 1), including the open circuit photovoltage (V_{oc}), short-circuit current (J_{sc}) and fill factor (FF). The best cell conversion efficiency of 16.9% is achieved with the PSC using 8 mg/mL PVK, which is much higher than that of the bare spiro-OMeTAD-based solar cell (14.1%). Further increase of the PVK concentration to 12 and 16 mg/mL leads to gradual decrease of PCE. This concentration-dependent trend in performance is in good agreement with above mentioned morphological evolution of the PVK films on top of perovskite, implying that an optimal PVK interlayer can not only suppress the electron recombination from the conduction band of TiO₂ to HTMs for avoiding direct contact between TiO₂ and HTM layer through traps, but also facilitate efficient charge separation and transportation owing to modulation

of perovskite-HTM interface. To testify this speculation, photoluminescence (PL) spectroscopy is employed to study the interfacial charge transfer processes. As seen in Fig. S3a, the bare perovskite film shows an intense PL peak at around 785 nm, which dramatically decreases after formation of perovskite/HTM layers due to hole injection from perovskite to spiro-OMeTAD. Further quenching of this emission is evident upon introduction of PVK interlayer, reaching the largest quenching effect at 8 mg/mL PVK coating concentration. These findings indicate improved exciton dissociation and more efficient charge transport among the perovskite/PVK/spiro-OMeTAD interfaces. Such PVK-facilitated interfacial charge transfer is also supported by the time-resolved PL decay measurements (Fig. S3b and Table S1), which reveal the same decay time downtrend as quenching effect, consistent with above concentration-dependent PVK film morphologies and cell performance. It is noteworthy that a negligible efficiency of 0.004% is observed if just employing PVK as HTM, suggesting PVK itself is not competent for charge transport. Ultraviolet photoelectron spectroscopy (UPS) was used to probe the HOMO energy level of the thin perovskite film, perovskite/PVK layer, and PVK film.⁴³ The HOMO values of the perovskite/PVK layer (-5.55 eV) and PVK film (-5.59 eV) are both lower than the valence band of perovskite (-5.43 eV), which is unfavourable for hole extraction (Fig. S4). This observation implies the faster hole transport mechanism through a thin film at the interface between PVK and HTM can have no relation to the energy levels of the polymer film. Moreover, direct doping of spiro-OMeTAD with PVK (e.g. 10 wt%) as a composite HTM layer only affords a lower efficiency of 12.9% relative to pure spiro-OMeTAD, suggestive of a deleterious effect. Based on these results, we conclude that the PVK-protecting interlayer is also useful, besides moisture resistance, to enhance overall PCE of PSCs *via* an optimized perovskite/PVK/HTM fabrication method.

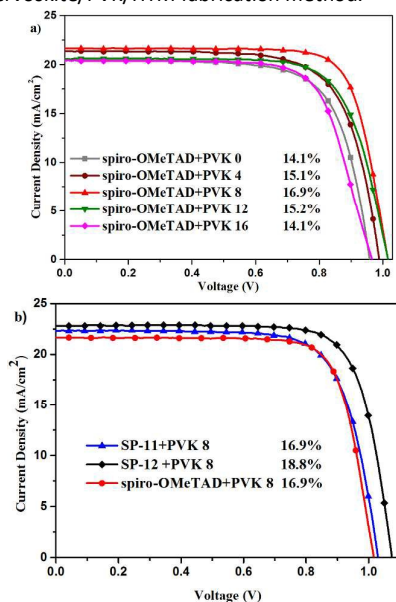


Fig. 4 *J-V* curves of PSCs prepared at different PVK concentrations with spiro-OMeTAD as HTM (a), and PSCs with optimal PVK interlayer and **SP-11**, **SP-12** and spiro-OMeTAD HTMs (b).

Table 1 PSC performance parameters extracted from *J-V* curves.^a

HTM	PVK (mg/mL)	J_{sc} (mA/cm ²)	V_{oc} (mV)	FF	η (%)
spiro-OMeTAD	0	20.6	958	0.71	14.1
spiro-OMeTAD	4	21.4	989	0.72	15.1
spiro-OMeTAD	8	21.6	1016	0.77	16.9
spiro-OMeTAD	12	20.6	1015	0.73	15.2
spiro-OMeTAD	16	20.4	966	0.72	14.1
PVK	8	0.06	254	0.28	0.004
10 wt% PVK + spiro-OMeTAD mixture	-	18.7	995	0.69	12.9
SP-11	0	19.8	978	0.72	13.9
SP-12	0	21.4	1000	0.73	15.5
SP-11	8	22.3	1030	0.74	16.9
SP-12	8	22.8	1075	0.77	18.8

^aUnder standard 100 mW cm⁻² AM 1.5 G solar illumination.

In order to check if the PVK-protection method is effective for generalization, we design two new triazatruxene-based HTMs, **SP-11** and **SP-12**, as shown in Fig. 1. Different from the reported triazatruxene analogs,³¹⁻³² we engineer a 2,7,12-substituted triazatruxene model to incorporate different donor branches and short ethyl groups into aromatic core. Thanks to PVK interlayer, long hydrophobic alkyl chains are no longer required to diminish their influence on conjugated π -system planarity and interfacial contact order. **SP-11** and **SP-12** were prepared by a facile synthetic route through Suzuki coupling reactions of readily available 2-BR-TAT⁴⁴ with 4-(4,4,5,5-tetramethyl-1,3,2-dioxaborolan-2-yl)-N,N-bis(4-methoxyphenyl)-aniline (**SP-11**, 86% yield) and *p*-methoxybenzene boronic acid (**SP-12**, 72% yield). Their chemical structures have been identified by virtue of ¹H/¹³C NMR spectroscopy, MALDI-TOF mass spectrometry and elemental analyses (details described in the Supporting Information).

The thermogravimetric analysis (TGA) and differential scanning calorimetry (DSC) studies unveil good thermal stability of **SP-11** and **SP-12** comparable with spiro-OMeTAD (Fig. S5-6), of which TGA curves indicate thermal decomposition at about 420 °C and DSC data show a higher glass transition temperature ($T_g = 125$ °C) of **SP-12** than that of **SP-11** ($T_g = 98$ °C). The normalized absorption and PL spectra in CH₂Cl₂ (Fig. S7) disclose that **SP-11**, **SP-12** and spiro-OMeTAD have maximum absorption peaks at 367, 340, and 387 nm and major emission peaks at 439, 423, and 428 nm, respectively. Largest Stokes shift is found for **SP-12**, implying that the small **SP-12** molecule could undergo significant geometrical change upon excitation, in favor of hole-transfer in solar cells.⁴⁵ The intersection wavelengths for **SP-11**, **SP-12** and spiro-OMeTAD are 410, 388, and 413 nm, which correspond to optical bandgaps (E_g) of 3.02, 3.19, and 3.00 eV, respectively.

Molecular orbital calculations of **SP-11** and **SP-12** are performed by TD-DFT program at B3LYP/3-21G* level to mimic their electronic structures. The HOMOs of two HTMs are found to delocalize over the whole molecule, while the LUMOs are mainly located on the linking phenyl rings (Fig. S8). The experimental HOMO levels of **SP-11**, **SP-12** and spiro-OMeTAD were derived from cyclic voltammetry (CV) measurements (Fig. S9). Three HTMs exhibit quasi-reversible redox peaks in CV, indicative of good electrochemical stability. The

HOMO levels of **SP-11** and **SP-12**, calculated as 5.34 and 5.41 eV from the first oxidation potentials, are lower than that of spiro-OMeTAD (-5.22 eV), but higher and closer to the valence band of perovskite (-5.43 eV). Therefore, relatively high open circuit voltage (V_{oc}) values are anticipated, especially for **SP-12**. An energy level diagram of the relevant materials is shown in Fig. 5, from which we can see that all HTMs have enough over potential to lead to efficient photo-generated charge transfer through the interfaces.

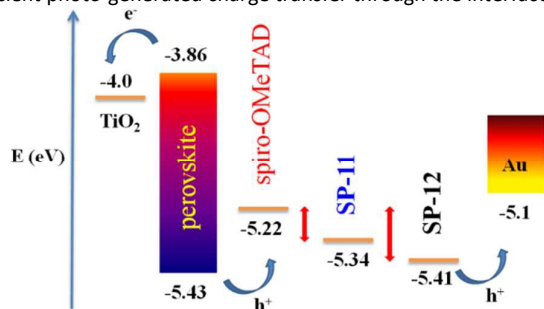


Fig. 5 The relative energy level diagram of relevant HTMs.

To understand the charge-carrier transport property, their hole transporting mobilities were evaluated by space charge limited current (SCLC) measurement. The hole mobility (μ) follows the order of μ_{SP-12} ($2.41 \times 10^{-4} \text{ cm}^2 \text{ V}^{-1} \text{ s}^{-1}$) $>$ μ_{SP-11} ($9.45 \times 10^{-5} \text{ cm}^2 \text{ V}^{-1} \text{ s}^{-1}$) $>$ $\mu_{\text{spiro-OMeTAD}}$ ($8.38 \times 10^{-5} \text{ cm}^2 \text{ V}^{-1} \text{ s}^{-1}$). The hole transporting capability of **SP-11** and **SP-12** as HTMs in PSCs is also estimated by PL spectra of perovskites underneath (Fig. S10). The remarkable diminution of PL intensity in the presence of HTMs confirms efficient hole injection from the valence band of perovskite into the HOMO of HTM. The PL quenching effect follows an order of **SP-12** $>$ **SP-11** $>$ spiro-OMeTAD, which indicates that carriers created in the excited perovskite layers are more efficiently extracted by triazatruxene-based HTMs, especially for **SP-12**. Faster hole injection rate of **SP-11** and **SP-12** than that of spiro-OMeTAD is also evident from the time-resolved PL measurements (Table S2). The relatively long life time of pristine perovskite decreases dramatically after incorporation of the HTMs, and the averaged decay times follow a similar order and is thus in accordance with the PL quenching results of perovskite containing three HTMs. Therefore, it can be concluded that the hole extraction and charge dissociation from perovskite to triazatruxene-based HTMs should be more efficient as compared to spiro-OMeTAD. Indeed, the PSC performance with **SP-11** as bare HTM (PCE = 13.9%) is comparable with spiro-OMeTAD (PCE = 14.1%) under the same conditions, while **SP-12** offers a higher PCE of 15.5% (Fig. S11 and Table 1).

To evaluate the performance of PVK-protected PSCs containing **SP-11** and **SP-12** as HTMs, similar planar PSC structure of FTO/compact-TiO₂/CH₃NH₃PbI₃/PVK/HTM/Au as above is adopted by replacing spiro-OMeTAD with the alternative HTM and incorporating an optimized PVK interlayer. The J - V curves of thus fabricated PSCs are illustrated in Fig. 4b and detailed parameters summarized in Table 1. The **SP-12**-based device exhibits PCE of 18.8%, higher than 16.9% of spiro-OMeTAD-based PSC containing PVK interlayer. The reverse scans of the PVK-protected PSCs are also performed, which give rise to slightly lower PCE due to the known hysteretic behavior (Fig. S11c and Table S3). The

measurements over 20 **SP-12**-based devices offer an average PCE value of $18.0 \pm 2.0\%$ (Fig. S12). It is noticeable that both the V_{oc} and J_{sc} values in **SP-12**-based PSC are enhanced relative to spiro-OMeTAD-based one, although their FF values are resembling, implying **SP-12** is an excellent alternative HTM of spiro-OMeTAD and especially suitable for this PVK-protection approach. In comparison, the **SP-11**-based PSCs achieve the same PCEs as the spiro-OMeTAD-based reference, of which the V_{oc} and J_{sc} values are also enhanced but the FF is lower, suggesting a poorer film quality with **SP-11**. The better V_{oc} and J_{sc} in both **SP-11**- and **SP-12**-based PSCs may be attributed to their deeper HOMO energy level and more efficient charge transfer, in agreement with the CV and PL results. This makes the triazatruxene-based HTMs promising lead structures for further molecular engineering. Moreover, the incident photon to current conversion efficiency (IPCE) spectra of all devices show similar profile ranging from 400 to 750 nm with a maximum at ca. 520 nm (Fig. S10). Compared with spiro-OMeTAD-based PSCs, **SP-11**- and **SP-12**-based PSCs display slightly higher IPCE throughout the broad range, consistent with the J - V measurements. The integrated J_{sc} values based on IPCE match well those from J - V curves (Fig. S13).

The protection effect of PVK on device stability has been investigated by aging control experiments of spiro-OMeTAD- and **SP-12**-based PSCs with or without PVK interlayer under identical conditions (ca. 35% humid atmosphere at room temperature). As seen from Fig. 6 and Fig. S14, the PCEs of pristine PSCs with bare spiro-OMeTAD and **SP-12** HTMs retain 68% and 73% of their initial efficiencies after 700 h, respectively. In contrast, the corresponding devices incorporating PVK interlayer lose their efficiency much more slowly, exhibiting retention of 87% and 90%, respectively. It is clear that the performance of PVK-protected devices has better durability against degradation, confirming that the PVK interlayer can effectively slow down the penetration of moisture into the perovskite layer. Moreover, **SP-12**-based devices present superior efficiency and stability relative to spiro-OMeTAD-based devices throughout the aging test, no matter in presence of PVK interlayer or not, justifying the quality and capability of **SP-12** as excellent HTM for PSCs.

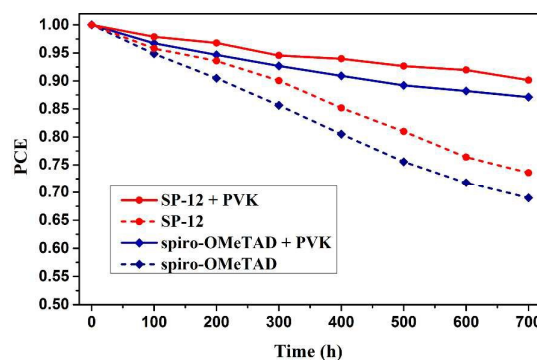


Fig. 6 The aging test comparison of spiro-OMeTAD- and **SP-12**-based PSCs with or without PVK interlayer.

Conclusions

In summary, a polymer-protection approach is demonstrated for PSC fabrication process by using hydrophobic and conductive PVK as a dual-functional interlayer to shield perovskite from moisture, suppress charge combination, and promote hole transport simultaneously. The concentration-dependent PVK-protection effect has been studied, revealing that the optimization of PVK interlayer for enhancement of device stability and performance is correlated with the film morphology. A new type of triazatruxene-based **SP-11** and **SP-12** HTMs is designed, available via a facile synthetic route for practice of this PVK-protection method. **SP-12** is proven to be an excellent small and simple molecular HTM candidate featuring suitable HOMO level and efficient charge transfer ability. Remarkable PCE exceeding 18% is realized using **SP-12** as HTM and PVK as interlayer, surpassing that of spiro-OMeTAD (16.9%). Superior stability against cell degradation has been verified for the proposed protection method. Interestingly, although the energy levels between perovskite and PVK are not matched, the PCEs of this device are magically increased owing to less charge combination and faster hole transport. This surprising phenomenon implies that other similar polymers could be effective for generalization as a functional interlayer to improve the efficiencies of PSCs. This interlayer between perovskite and HTM could be a promising avenue for the PSC architecture and open a new direction of process development for highly efficient and stable PSCs. Further advancement is expected *via* optimizing polymer interlayer, HTM structure and processing conditions.

Acknowledgements

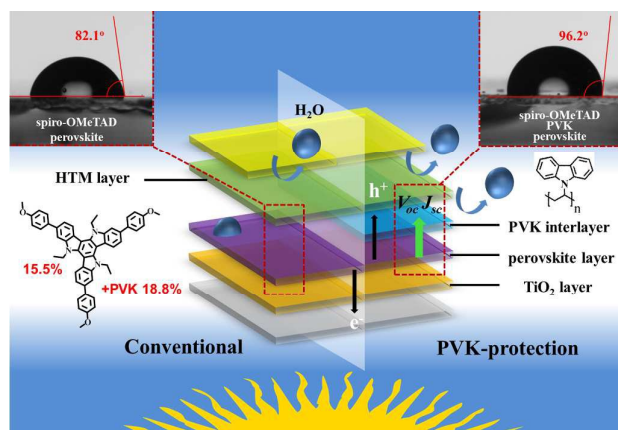
This work was supported by the NSFC Projects (91222201, 21572280, 61370059, 21573291), STP Project of Guangzhou (15020016), NSF of Beijing (4152030) and NSF of Guangdong Province (S2013030013474).

References

- A. Kojima, K. Teshima, Y. Shirai, T. Miyasaka, *J. Am. Chem. Soc.*, 2009, **131**, 6050-6051.
- W. S. Yang, J. H. Noh, N. J. Jeon, Y. C. Kim, S. Ryu, J. Seo, S. I. Seok, *Science*, 2015, **348**, 1234-1237.
- D. Bi, W. Tress, M. I. Dar, P. Gao, J. Luo, C. Renevier, K. Schenk, A. Abate, F. Giordano, J.-P. Correa-Baena, J.-D. Decoppet, S. M. Zakeeruddin, M. K. Nazeeruddin, M. Grätzel, A. Hagfeldt, *Sci. Adv.*, 2016, **2**, 1501170.
- A. Krishna, D. Sabba, J. Yin, A. Bruno, L. J. Antila, C. Soci, S. Mhaisalkar, A. C. Grimsdale, *J. Mater. Chem. A*, 2016, **4**, 8750-8754.
- S. Ma, H. Zhang, N. Zhao, Y. Cheng, M. Wang, Y. Shen, G. Tu, *J. Mater. Chem. A*, 2015, **3**, 12139-12144.
- M. Z. Liu, M. B. Johnston, H. J. Snaith, *Nature*, 2013, **501**, 395-398.
- H. J. Jeon, J. H. Noh, W. S. Yang, Y. C. Kim, S. Ryu, J. Seo, S. I. Seok, *Nature*, 2015, **517**, 476-480.
- Z. Yu, L. Sun, *Adv. Energy Mater.*, 2015, 1500213-1500230; c) X. Li, D. Bi, C. Yi, J.-D. Decoppet, J. Luo, S. M. Zakeeruddin, A. Hagfeldt, M. Grätzel, *Science*, 2016, **353**, 58-62.
- H. S. Rao, B. X. Chen, W. G. Li, Y. F. Xu, H. Y. Chen, D. B. Kuang, C. Y. Su, *Adv. Funct. Mater.*, 2015, **25**, 7200-7207.
- K. Rakstys, M. Saliba, P. Gao, P. Gratia, E. Kamaraukas, S. Paek, V. Jankauskas, M. K. Nazeeruddin, *Angew. Chem. Int. Ed.*, 2016, **55**, 7464-7468; *Angew. Chem.*, 2016, **128**, 7590-7594.
- Y. Liu, Q. Chen, H. -S. Duan, H. Zhou, Y. (M.) Yang, H. Chen, S. Luo, T. -B. Song, L. Dou, Z. Hong, Y. Yang, *J. Mater. Chem. A*, 2015, **3**, 11940-11947.
- T. Swetha, S. P. Singh, *J. Mater. Chem. A*, 2015, **3**, 18329-18344.
- W. Chen, Y. Wu, J. Liu, C. Qin, X. Yang, A. Islam, Y. -B. Cheng, L. Han, *Energy Environ. Sci.*, 2015, **8**, 629-640.
- Y. Han, S. Meyer, Y. Dkhissi, K. Weber, J. M. Pringle, U. Bach, L. Spiccia, Y. -B. Cheng, *J. Mater. Chem. A*, 2015, **3**, 8139-8147.
- M. L. Petrus, T. Bein, T. J. Dingemans, P. Docampo, *J. Mater. Chem. A*, 2015, **3**, 12159-12162.
- M. Cai, V. T. Tiong, T. Hreid, J. Bell, H. Wang, *J. Mater. Chem. A*, 2015, **3**, 2784-2793.
- C. H. The, R. Daik, E. L. Lim, C. C. Yap, M. A. Lbrahim, N. A. Ludin, K. Sopian, M. A. M. Teridi, *J. Mater. Chem. A*, 2016, Advance Article.
- B. Xu, E. Sheibani, P. Liu, J. Zhang, H. Tian, N. Vlachopoulos, G. Boschloo, L. Kloo, A. Hagfeldt, L. Sun, *adv. Mater.*, 2014, **26**, 6629-6634.
- C. C. Stoumpos, C. D. Malliakas, M. G. Kanatzidis, *Inorg. Chem.*, 2013, **52**, 9019-9038.
- J. Burschka, N. Pellet, S.-J. Moon, R. Humphry-Baker, P. Gao, M. K. Nazeeruddin, M. Grätzel, *Nature*, 2013, **499**, 316-319.
- N. Ahn, D.-Y. Son, I.-H. Jang, S. M. Kang, M. Choi, N.-G. Park, *J. Am. Chem. Soc.*, 2015, **137**, 8696-8699.
- S. D. Stranks, P. K. Nayak, W. Zhang, T. Stergiopoulos, H. J. Snaith, *Angew. Chem. Int. Ed.*, 2015, **54**, 3240-3248; *Angew. Chem.*, 2015, **127**, 3288-3297.
- S. N. Habisreutinger, T. Leijtens, G. E. Eperon, S. D. Stranks, R. J. Nicholas, H. J. Snaith, *Nano Lett.*, 2014, **14**, 5561-5568.
- M. Grätzel, *Nat. Mater.*, 2014, **13**, 838-842.
- I. C. Smith, E. T. Hoke, D. Solis-Ibarra, M. D. McGehee, H. I. Karunadasa, *Angew. Chem. Int. Ed.*, 2014, **53**, 11232-11235; *Angew. Chem.*, 2014, **126**, 11414-11417.
- L.-L. Zheng, Y.-H. Chung, Y. Ma, L. Zhang, L. Xiao, Z. Chen, S. Wang, B. Qu, Q. Gong, *Chem. Commun.*, 2014, **50**, 11196-11199.
- D. Bi, A. Mishra, P. Gao, M. Franckevičius, C. Steck, S. M. Zakeeruddin, M. K. Nazeeruddin, P. Bäuerle, M. Grätzel, A. Hagfeldt, *ChemSusChem*, 2016, **9**, 433-438.
- Z. Yu, L. Sun, *Adv. Energy Mater.*, 2015, **5**, 1500213-1500229.
- S. Ryu, J. H. Noh, N. J. Jeon, Y. C. Kim, W. S. Yang, J. Seo, S. I. Seok, *Energy Environ. Sci.*, 2014, **7**, 2614-2618.
- A. Mei, X. Li, L. Liu, Z. Ku, T. Liu, Y. Rong, M. Xu, M. Hu, J. Chen, Y. Yang, M. Grätzel, H. Han, *Science*, 2014, **345**, 295-298.
- K. Rakstys, A. Abate, M. I. Dar, P. Gao, V. Jankauskas, G. Jacopin, E. Kamaraukas, S. Kazim, S. Ahmad, M. Grätzel, M. K. Nazeeruddin, *J. Am. Chem. Soc.*, 2015, **137**, 16172-16178.
- F. J. Ramos, K. Rakstys, S. Kazim, M. Grätzel, M. K. Nazeeruddin, S. Ahmad, *RSC Adv.*, 2015, **5**, 53426-53432.
- J. -H. Im, C. -R. Lee, J. -W. Lee, S. -W. Park, N. -G. Park, *Nanoscale*, 2011, **3**, 4088-4093.
- H. -S. Kim, J. -W. Lee, N. Yantara, P. P. Boix, S. A. Kulkarni, S. Mhaisalkar, M. Mratzel, N. -G. Park, *Nano Lett.*, 2013, **13**, 2412-2417.
- G. Niu, W. Li, F. meng, L. Wang, H. Dong, Y. Qiu, *J. Mater. Chem. A.*, 2014, **2**, 705-710.
- O. Ostroverkhova, W. E. Moerner, *Chem. Rev.*, 2004, **104**, 3267-3314.

- 37 J. L. Maldonado, Y. Ponce-de-Leon, G. Ramos-Ortiz, M. Rodriguez, M. A. Meneses-Nava, O. Barbosa-Garcia, R. Santillan, N. Farfan, *J. Phys. D Appl. Phys.*, 2009, **42**, 075102.
- 38 V. -M. Herrera-Ambriz, J. L. Maldonado, M. Rodrigue, R. Castro-Beltran, G. Ramos-Ortiz, N. -E. Magana-Vergara, M. -A. Meneses-Nava, O. Barbosa-Garcia, R. Santillan, N. Farfan, F. -X. Dang, P. G. Lacroix, I. Ledoux-Rak, *J. Phys. Chem. C.*, 2011, **115**, 23955-23963.
- 39 L. Sicot, C. Fiorini, A. Lorin, P. Raimond, C. Sentein, J. -M. Nunzi, *Sol. Energy Mater. Sol. Cells*, 2000, **63**, 49-60.
- 40 H. -S. Kim, C. -H. Kim, C. -S. Ha, J. -K. Lee, *Synth. Met.*, 2001, **117**, 289-291.
- 41 T. -H. Zhang, S. -L. Zhao, L. -Y. Piao, Z. Xu, S. -T. Ju, X. -D. Liu, C. Kong, X. -R. Xu, *Chin. Phys. B*, 2011, **20**, 038401.
- 42 P.-Y. Su, Y.-F. Chen, J.-M. Liu, L.-M. Xiao, D.-B. Kuang, M. Mayor, C.-Y. Su, *Electrochimica Acta*, 2016, **209**, 529-540.
- 43 M. T. Greiner, M. G. Helander, W. M. Tang, Z. B. Wang, J. Qiu, Z. H. Lu, *Nat. Mater.*, 2012, **11**, 76-81.
- 44 Y.-F. Xie, S.-Y. Ding, J.-M. Liu, W. Wang, Q.-Y. Zheng, *J. Mater. Chem. C*, 2015, **3**, 10066-10069.
- 45 D.-H. Lee, Y.-P. Liu, K.-H. Lee, H. Chae, S. M. Cho, *Org. Electron.*, 2010, **11**, 427-433.

Table of Contents Entry



Cooperation of polymer-protection method with molecular design of a novel HTM in PSCs: a PVK-protection approach is proposed to improve cell efficiency and stability, for practice of which a low-cost triazatruxene-based HTM is developed. This work opens a new avenue for development of highly efficient and stable PSCs.